SUPPLEMENTARY INFORMATION

# CONTACT ANGLE AND ADSORPTION ENERGIES OF NANOPARTICLES AT THE AIR-LIQUID INTERFACE DETERMINED BY NEUTRON REFLECTIVITY AND MOLECULAR DYNAMICS

Javier Reguera[a,b,c*], Evgeniy Ponomarev[a], Thomas Geue[d], Francesco Stellacci[a], Fernando Bresme[e*], Mauro Moglianetti[f*]

[a] Institute of Materials, École Polytechnique Fédérale de Lausanne, 1015 Lausanne, Switzerland
[b] CIC biomaGUNE, Paseo de Miramón 182, 20009 Donostia-San Sebastian, Spain
[c] Ikerbasque, Basque Foundation for Science, 48011 Bilbao, Spain
[d] Laboratory for Neutron Scattering and Imaging, Paul Scherrer Institut, 5232 Villigen, Switzerland
[e] Department of Chemistry, Imperial College, SW7 2AZ, London, United Kingdom
[f] Center for Biomolecular Nanotechnologies (CBN), Istituto Italiano di Tecnologia, 73010 Arnesano, Italy

## Index

# 1. TEM images

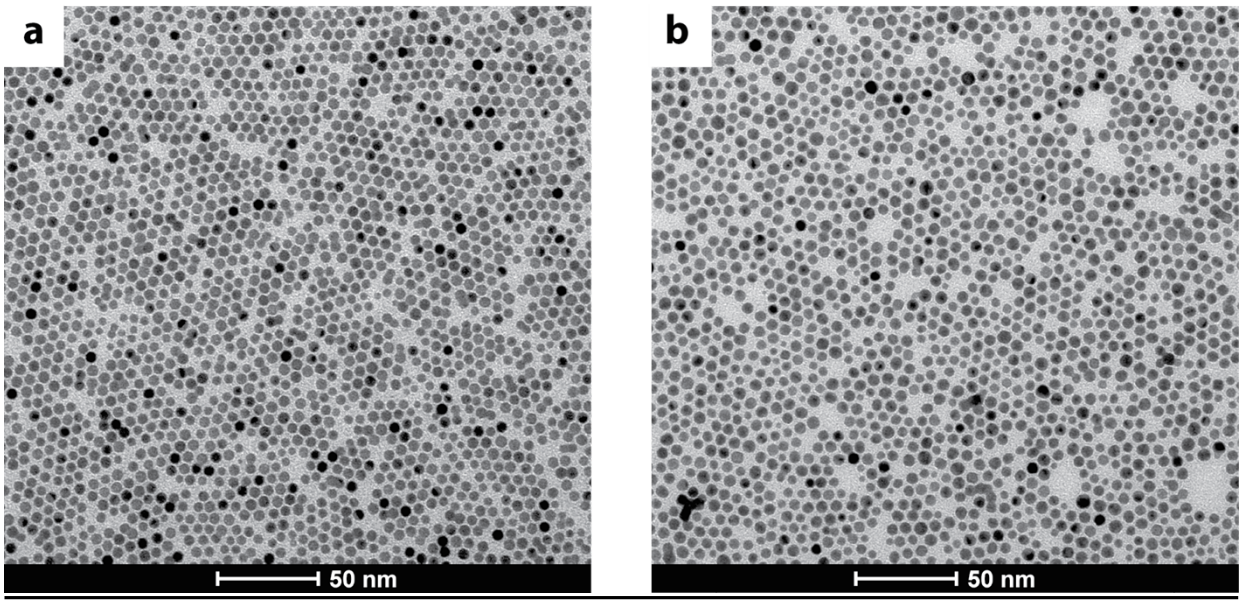


**Figure S1**: TEM image of a NP monolayer. **a)** dOT covered NPs obtained using Langmuir-Schaefer on water subphase with null scattering length density. b) dOT:MHol 1:1 covered NPs obtained using Langmuir-Schaefer on water subphase with the scattering length density of gold.

# 2. Model of nanoparticles monolayer for neutron reflectivity

## 2.1 General description and modeling of the core

The model input parameters determined experimentally in this paper are the average diameter of nanoparticles $d_{av}$, its standard deviation $\sigma_d$, average distance between nanoparticles' edges $ed_{av}$ and its standard deviation $\sigma_{ed}$. Furthermore, values of following parameters were obtained from the literature: $L_{lig}$ is length of ligand molecule; $\beta^{core}$, $\beta^{shell}$ and $\beta^{subphase}$ are scattering length densities of gold core, ligand shell and subphase respectively. The only parameter that was varied to fit the data is immersion depth (*id*) of the size-averaged nanoparticle into the subphase. For each fitting process, the value of contact angle $\Theta$ is initially set and corresponding values of immersion depth are calculated for particles of different diameters in order to keep the same contact angle (Fig.1b). Difference in immersion depth is expected due to the intrinsic polydispersity of the NPs (Fig.S2).

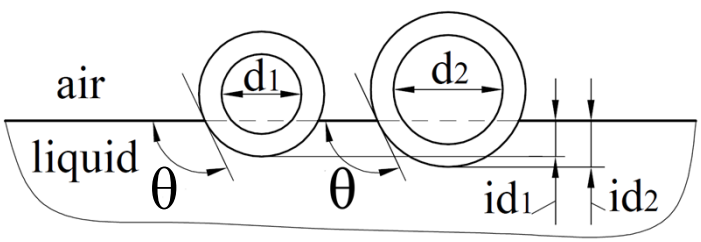


**Figure S2.** Cartoon showing an example of two nanoparticles with the same contact angle. Due to the polydispersity of the sample, different particles will show different diameters and therefore different immersion depths.

Gaussian distribution was used to model size distribution of nanoparticles:

$$f(x) = \frac{\exp\left(\frac{-(x-d_{av})^2}{2\cdot\sigma_d^2}\right)}{\sigma_d\cdot\sqrt{2\pi}} \quad (s1)$$

Two-dimensional array **Sz** with P rows and 2 columns was generated in order to represent this distribution. Element Sz [i,1] is the number of particles with diameter Sz[i,2] and is equal to Sz[i,1]= Int(100·f(Sz[i,2])), where i is an arbitrary element of this array and Int() is an operator which gives an integer part of number. Thus, a system of $N_{total} = \sum_{i=1}^{P} Sz\,[i,1]$ particles was created (for OT $N_{total}$ = 987, for OT-Mhol $N_{total}$ = 967). For distances between nanoparticles edges, one-dimensional array **Ed** of length P was created. Values of elements of this array are equally distributed in the interval between $ed_{av} - 2\sigma_{ed}$ and $ed_{av} + 2\sigma_{ed}$.

The monolayer of nanoparticles was divided into N horizontal sublayers with thickness of 1 Å. Interface-normal scattering length density for layer n is defined as:

$$\rho_n = \sum_{i=1}^{P} Fr_i(d_{av},\sigma_d;d_i)\cdot\left(\beta_{shell}\frac{A_i^{shell}}{A_i^{cell}} + \beta_{core}\frac{A_i^{core}}{A_i^{cell}} + \beta_{subphase}\frac{A_i^{subphase}}{A_i^{cell}}\right) \quad (s2)$$

where $d_i$ = Sz[i,2] is the diameter of i-th particle; $Fr_i$ is a fraction of nanoparticles with diameter $d_i$ defined as $Fr_i(d_{av},\sigma_d;d_i) = \frac{Sz[i,1]}{N_{total}}$; $A_i^{cell}$ is area of a unit cell in the hexagonal lattice which correspond to i-th particle; $A_i^{shell}$, $A_i^{core}$, $A_i^{subphase}$ are areas which are occupied by shell, core and subphase in the n-th slab respectively. Total scattering length density profile of the whole monolayer is defined as:

$$R(z) = \sum_{n=1}^{N} \rho_n \quad (s3)$$

**Area of unit cell** is equal to

$$A_i^{cell}(Sz[i,2],Ed[i]) = (Sz[i,2] + Ed[i])^2\cdot\sin 60° \quad (s4)$$

**Area occupied by gold core**

$A_i^{core}$ is a function of nanoparticle diameter and corresponding z coordinate (Fig.1b). For a particle with diameter Sz[i,2] and value of z equal $z_j$ $A_i^{core}$ is determined as a cross section of spherical gold core along the dashed line in Fig. S3. $Z_s$ is a coordinate of axis of symmetry of nanoparticle monolayer and values of $A_i^{core}$ are symmetric with respect to this axis. For simplicity, coordinate system is defined in the way that for each particle of diameter Sz[i,2] $z_s$ is equal to 0. In such system $A_i^{core}$ is equal to:

$$A_i^{core} = \begin{cases} 0, & z > R_c \\ \pi\cdot\left(R_c{}^2 - z^2\right), & -R_c \le z \le R_c \\ 0, & z < -R_c \end{cases} \quad (s5)$$

where the nanoparticle radius $R_c$ is equal to Sz[i,2]/2;

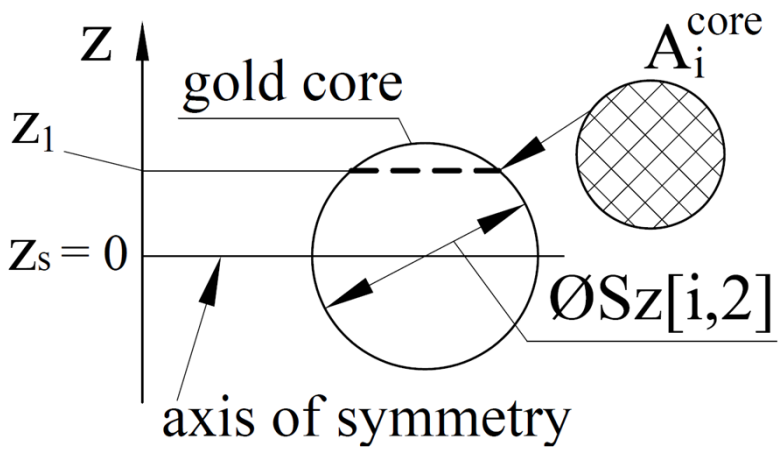


**Figure S3.** Drawing of the calculation of area occupied by gold core.

**Classification depending of the area occupied by ligands shell:**

## 2.2 Homoligand NPs

$A_i^{shell}$ is a function of nanoparticle diameter, interparticle distance and corresponding z coordinate. In this model gold core was considered as rigid non-compressible sphere while ligands shell was assumed to be laterally deformable. These assumptions are backed by our atomistic molecular dynamics simulations of model nanoparticles that match the experimental system. Depending on distance between nanoparticles edges three different cases of shell geometry were considered.

Case A1

For this case distance between nanoparticles edges is greater than $2 \cdot L_{lig}$ and $A_i^{shell}$ is defined as a cross section of shell in the same way as $A_i^{core}$.

$$A_i^{shell} = \begin{cases} 0, & z > R_{shell} \\ \pi \cdot \left(R_{shell}^{\ 2} - z^2\right), & R_c < z \leq R_{shell} \\ \pi \cdot \left(R_{shell}^{\ 2} - R_c^{\ 2}\right), & -R_c \leq z \leq R_c \\ \pi \cdot \left(R_{shell}^{\ 2} - z^2\right), & -R_{shell} \leq z < -R_c \\ 0, & z < -R_{shell} \end{cases} \quad (s5)$$

where the shell radius $R_{shell}$ is equal to $R_c + L_{lig}$.

Case A2

Values of interparticle distances in this case are in the interval of $2 \cdot L_{lig} \cdot \cos 30^o - Sz[i,2] \leq ed < 2 \cdot L_{lig}$. The upper ($ed_1$) and the lower ($ed_2$) limits of this range correspond to geometry shown in Fig. S4a and Fig. S4b respectively where the top view of nanoparticle monolayer is represented. As the interparticle distance decreases the ligand shell starts to compress. Cross section $A_i^{shell}$ for values of z where shells start to contact is defined by area confined by the shells of neighboring particles in hexagonal lattice (hatched area in Fig. S5). For the lower limit $ed_2$ the outer contour of $A_i^{shell}$ cross section for z=0 transforms into regular hexagon.

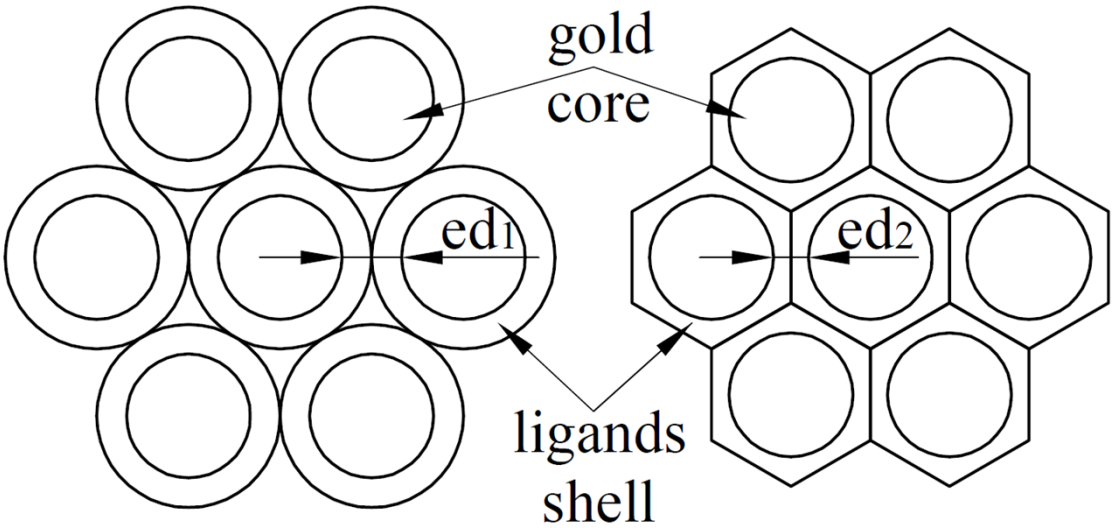


**Figure S4.** Geometry of nanoparticle monolayer (top view) for case A2.

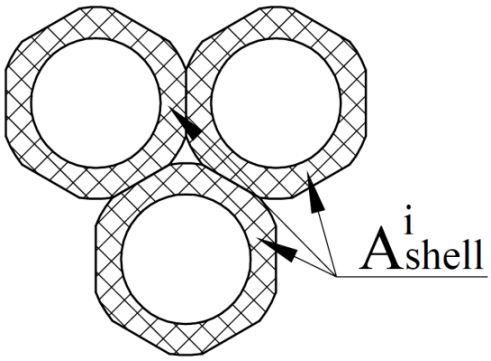


**Figure S5.** Cross section $A_i^{shell}$ for case A2.

$$A_i^{shell} = \begin{cases} 0, & z > R_{shell} \\ \pi\cdot\left(R_{shell}^2 - z^2\right), & R_c < z \le R_{shell} \\ \pi\cdot\left(R_{shell}^2 - R_c^2\right), & \sqrt{R_{shell}^2 - \left(R_c + \frac{ed}{2}\right)^2} < z \le R_c \\ \pi\cdot\left(R_{shell}^2 - R_c^2\right) - S, & -\sqrt{R_{shell}^2 - \left(R_c + \frac{ed}{2}\right)^2} \le z \le \sqrt{R_{shell}^2 - \left(R_c + \frac{ed}{2}\right)^2} \\ \pi\cdot\left(R_{shell}^2 - R_c^2\right), & -R_c \le z < -\sqrt{R_{shell}^2 - \left(R_c + \frac{ed}{2}\right)^2} \\ \pi\cdot\left(R_{shell}^2 - z^2\right), & -R_{shell} \le z < -R_c \\ 0, & z < -R_{shell} \end{cases} \quad (s6)$$

S is total intersection area between shell of particle and shells of its 6 neighbors in hexagonal cell and is equal to $S=6\cdot S_{segm}$(Fig. S6) where $S_{segm}$ is an area of circular segment defined in this case as:

$$S_{segm} = \frac{R_i^2}{2}\cdot(\alpha - sin\alpha)$$

$$R_i = {R_{shell}}^2 - z^2; \qquad \alpha = 2 \cdot arccos\left(\frac{R_c + \frac{ed}{2}}{R_i}\right)$$

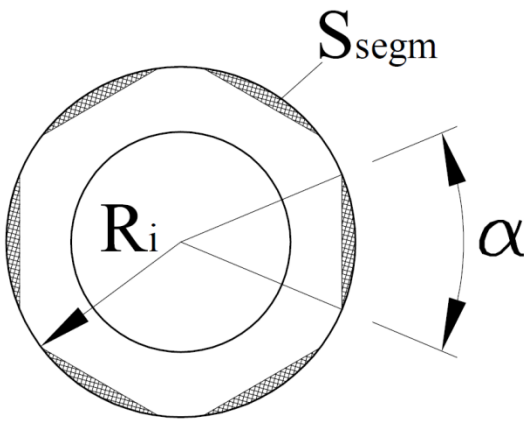


**Figure S6.** Area of circular segment $S_{segm}$ (hatched)

Case A3

For this case ed< $2 \cdot L_{lig} \cdot \cos 30^o$- Sz[i,2]. In the region of shell contact $A_i^{shell}$ cross section has two different shapes depending on value of z. For z in the range of $z_1$–$z_2$ the area of cross section correspond to $A_i^{shell,1}$ while for the range of $z_2$–$z_s$ – to $A_i^{shell,2}$ (Fig. S7).

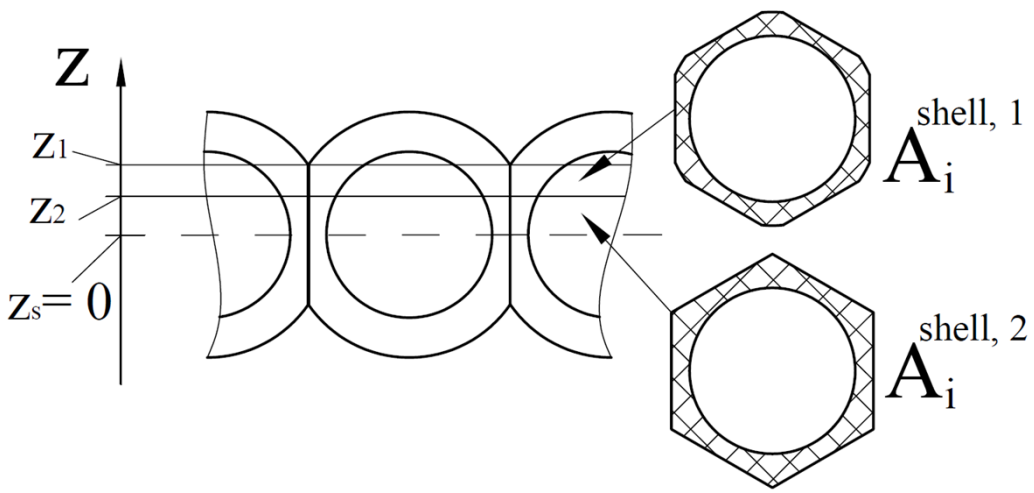


**Figure S7.** Area occupied by ligand shell for A3 case.

$$A_i^{shell} = \begin{cases} 0, & z > R_{shell} \\ \pi\cdot\left(R_{shell}{}^2 - z^2\right), & R_c < z \le R_{shell} \\ \pi\cdot\left(R_{shell}{}^2 - R_c{}^2\right), & \sqrt{R_{shell}{}^2 - \left(R_c + \frac{ed}{2}\right)^2} < z \le R_c \\ \pi\cdot\left(R_{shell}{}^2 - R_c{}^2\right) - S, & \sqrt{R_{shell}{}^2 - \left(\frac{R_c + 0.5\cdot ed}{cos30°}\right)^2} < z \le \sqrt{R_{shell}{}^2 - \left(R_c + \frac{ed}{2}\right)^2} \\ A_{hex} - \pi\cdot\left(R_c{}^2 - z^2\right), & -\sqrt{R_{shell}{}^2 - \left(\frac{R_c + 0.5\cdot ed}{cos30°}\right)^2} \le z \le \sqrt{R_{shell}{}^2 - \left(\frac{R_c + 0.5\cdot ed}{cos30°}\right)^2} \\ \pi\cdot\left(R_{shell}{}^2 - R_c{}^2\right) - S, & -\sqrt{R_{shell}{}^2 - \left(R_c + \frac{ed}{2}\right)^2} \le z \le -\sqrt{R_{shell}{}^2 - \left(\frac{R_c + 0.5\cdot ed}{cos30°}\right)^2} \\ \pi\cdot\left(R_{shell}{}^2 - R_c{}^2\right), & -R_c \le z < -\sqrt{R_{shell}{}^2 - \left(R_c + \frac{ed}{2}\right)^2} \\ \pi\cdot\left(R_{shell}{}^2 - z^2\right), & -R_{shell} \le z < -R_c \\ 0, & z < -R_{shell} \end{cases} \quad (s7)$$

where $A_{hex}$ is area of hexagon defined as $A_{hex} = \frac{3\sqrt{3}}{2}\left(\frac{R_c + 0.5\cdot ed}{cos30°}\right)^2$

### 2.3 Mixed ligands NPs

Nanoparticles coated with 2 types of ligands in the molar ratio 1:1 were studied. Values of length and scattering length density for hydrophobic and hydrophilic ligands are equal to $L_{lig}^1$ and $L_{lig}^2$ and $\beta_{lig}^1$ and $\beta_{lig}^2$ respectively.

Janus model

For the Janus model area of ligand shell $A_i^{shell}$ is calculated according to equations s5-s7 with value of $L_{lig} = L_{lig}^1$ for $z > 0$ and $L_{lig} = L_{lig}^2$ for $z \le 0$ (Fig. S8). Value of $\beta^{shell}$ is set to $\beta_{lig}^1$ for $z > 0$ and to $\beta_{lig}^2$ for $z \le 0$.

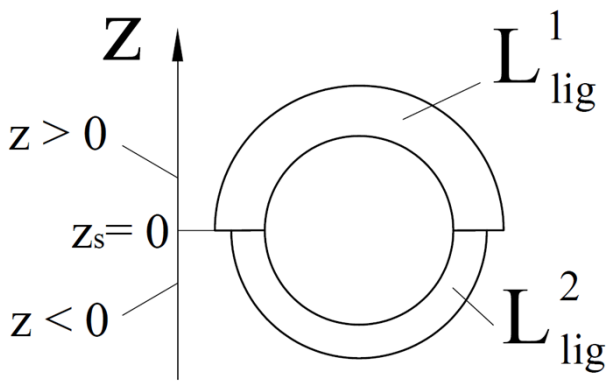


**Figure S8.** Janus model

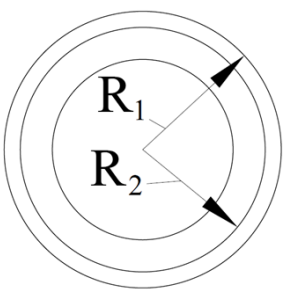


**Figure S9.** Uniformly mixed model

Uniformly mixed model

In this model $A_i^{shell}$ is defined for 2 volumes (fig. S9): the first one is confined between spheres of radii $R_1$=Rc+ $L_{lig}^1$ and $R_2$= Rc+ $L_{lig}^2$ and the second one – between $R_2$ and Rc.

For the first case:

$A_i^{shell} = 0.5 \cdot A_i^{shell\ homoligand}(L_{lig} = L_{lig}^1, \beta^{shell} = \beta_{lig}^1)$,

for the second case:

$A_i^{shell} = 0.5 \cdot A_i^{shell\ homoligand}(L_{lig} = L_{lig}^1, \beta^{shell} = \beta_{lig}^1) + 0.5 \cdot A_i^{shell\ homoligand}(L_{lig} = L_{lig}^2, \beta^{shell} = \beta_{lig}^2)$, where $A_i^{shell\ homoligand}$ is area of ligand shell of homoligand nanoparticle calculated according to equations s5-s7 with corresponding values of ligand length and scattering length density.

**Area occupied by subphase**

This area is defined as:

$$A_i^{subphase} = \begin{cases} 0, & z > -(R_{shell} - id_i) \\ A_i^{cell} - \left(A_i^{core} + A_i^{shell}\right), & -id_i < z \leq -(R_{shell} - id_i) \\ A_i^{cell}, & -id_{max} \leq z \leq -id_i \\ 0, & z < -R_{shell} \end{cases} \quad (s8)$$

where $id_i$ is immersion depth which corresponds to particle with diameter Sz[i,2]; $id_{max}$– immersion depth of particle with the largest diameter in considered system.

# 3. Fitting of Janus model for dOT:MHol 1:1 in CMAu

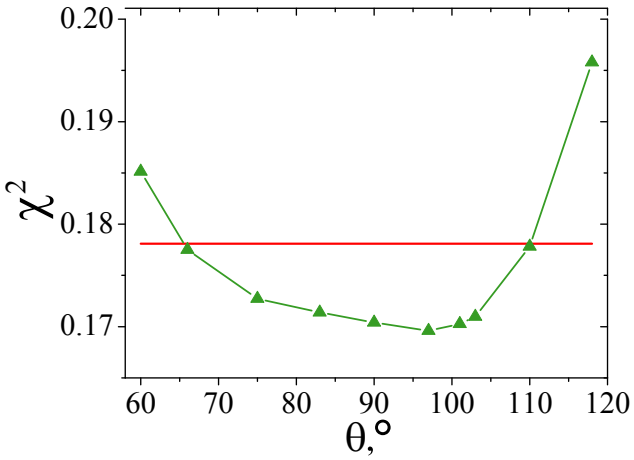


**Figure S10.** Fitting parameter $\chi^2$ as a function of contact angle for the contrast CMAu when using a Janus model on dOT-MHol NPs. The error of the angle indicated with the red line has to be chosen with $\chi^2=1.05\cdot \chi^2_{min}$.

**Table S1.** $\chi^2$ for Janus and uniformly mixed structures

| Contrast | Contact angle, ° | $\chi^2$ Janus structure | $\chi^2$ Uniformly mixed structure |
|---|---|---|---|
| CMAu | 118 | 0.1958 | 0.0176 |
| | 110 | 0.1778 | 0.0142 |
| | 103 | 0.1709 | 0.0127 |
| | 101 | 0.1702 | 0.0122 |
| | 97 | 0.1696 | 0.012 |
| | 90 | 0.1704 | 0.0116 |
| | 84 | 0.1738 | 0.0111 |
| | 75 | 0.1727 | 0.0116 |
| | 66 | 0.1775 | 0.0138 |
| | 60 | 0.1851 | 0.0172 |
| NRW | - | 0.1217 | 0.0121 |

# 4. Computer simulations of nanoparticles at the air-water interface

### 4.1 Single NPs at interfaces

Atomistic classical molecular dynamics simulations were performed to compute the contact angle of single nanoparticles and small arrays consisting of 7 nanoparticles. The nanoparticle core was constructed by cutting a spherical cluster from a gold bulk crystal consisting of atoms arranged in an fcc lattice with the experimental lattice parameter at 300 K. The radius used to cut the sphere was chosen to produce particles with a core radius matching our experimental measurements. We thus generated a gold core cluster containing 3832 with a diameter ~4.85 nm. For testing purposes we also generated another cluster with dodecahedral symmetry and containing 1289 gold atoms.

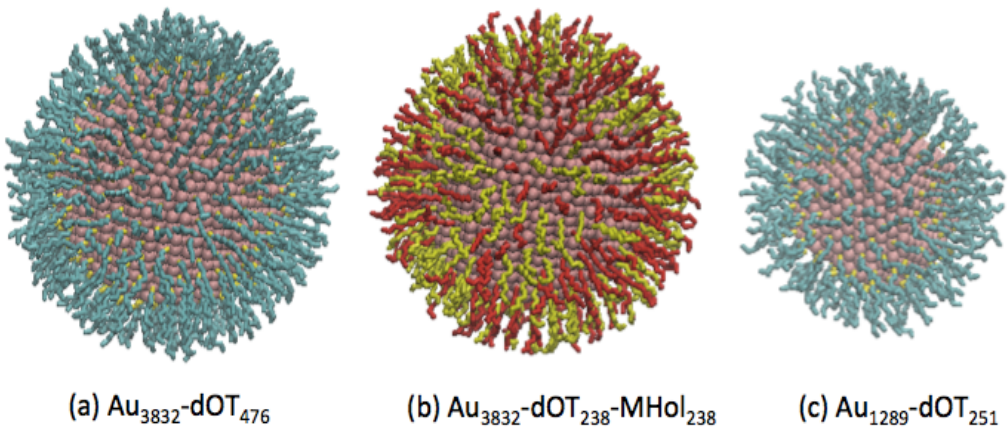


Figure S11: Gold nanoparticles simulated in this work. (a) Pure octanethiol, (b) equilmolar mixture of octanethiol (red) and 6-Mercapto-1-hexanol (yellow) and (c) pure octanethiol with smaller nanoparticle radius.

The functionalized thiol nanoparticles were constructed by immersing the clusters in cubic simulation box (3375 $nm^3$) containing a large excess of octanethiols (dOT), typically >2000 per particle. A canonical simulation was then performed for 3 ns (0.002 ps timestep) at 500 K to enable enough diffusion of the thiols. After this initial process the simulation temperature was reduced to 300 K and the system simulated for a further ns. We then eliminated all the alkanethiols that were not in direct contact with the cluster. A cutoff criterion was used with this purpose such that any alkanethiol whose sulfur atom was lying beyond 0.34 nm was discarded. This distance corresponds to the minimum in the Au-S radial distribution function and it ensures that we consider all the thiol molecules adsorbed in the cluster. Once the excess molecules were removed, we performed an additional equilibration for 2 ns, to enable the detachment of any extra thiols weakly adsorbed at the gold particle. This simulation protocol produced $Au_{3832}$-$dOT_{476}$ and $Au_{1289}$-$dOT_{251}$ NPs. In order to generate the 50:50 6-mercapto-1-hexanol:dOT functionalized nanoparticles ($Au_{3832}$-$dOT_{238}$-$MHol_{238}$), we replaced the terminal $CD_2$-$CD_3$ groups in dOT by an O-H. We note that there are no specific force-fields in the literature that model deuterium. Hence we adopted pair interactions used to model $CD_3$ and $CD_2$ groups within the united atom approach. Notice that not a significant difference is expected between the hydrogenous and the deuterated groups. dOT molecules were chosen randomly in order to render a homogeneous distribution of ligands. We show in Fig. S11 the three nanoparticles simulated in this work.

The particle interactions were modelled with a combination of intermolecular (dispersions interactions modelled with the Lennard-Jones potential) and intramolecular interactions. The general functional form of the forcefields has been described in reference[1,2]. The gold-gold interactions in this work were

modelled using strong Lennard-Jones potentials with the minimum of the potential set to the Au-Au distance in the nanoparticle and the interaction strength was scaled to 150 kJ/mol to ensure the cluster integrity. The dOT thiols were modelled using the parameters reported in reference[1] while the OH group in the 6-mercapto-1-hexanol was modeled with the TraPPE forcefield.[3] In order to model the water surface, we employed the TIP4P/2005 water model,[4] which provides an accurate representation of the thermodynamic properties of water in a wide range of temperatures, including its surface tension, which is a relevant property in the present investigation. Cross interactions between dissimilar groups were derived by applying standard combination rules and all the dispersion interactions were cutoff at 1.5 nm, while the electrostatic interactions were computed in full using the Particle Mesh Ewald method[5] and a 3D Ewald dipole correction[6] for the simulation of water interfaces. All the simulations were performed with GROMACS v. 4.5.5.[7] For the simulations of nanoparticle arrays consisting of 7 nanoparticles the inter-cluster gold-gold interactions were modelled with a weaker gold-gold interaction than the intramolecular ones, using the parameters reported in reference.[1] A typical simulation consisted of 185556 and 680260 particles for the isolated and arrays studies respectively, with simulation times of the order of 5 ns.

The simulations were started by placing the particle next to a pre-equilibrated water slab avoiding strong overlaps between particle and solvent atoms. After a transient period, typically ~1 ns, the nanoparticle landed on the water surface, and subsequent configurations were employed to compute the cylindrical density profile of the solvent and ligands in terms of the radial distance parallel to the water surface, *r*, and the height, z, in the direction perpendicular to the interface place.[1] These density profiles were employed to obtain contour plots that were later used to extract the contact angles (Note that *r* in NR model refers to the core radius). The standard error of the contact angle was calculated from 10 independent simulations.

Snapshot of the equilibrated NPs and angle calculations are shown in the main text for $Au_{3832}$-$dOT_{476}$ and $Au_{3832}$-$dOT_{238}$-$MHol_{238}$ and in Fig. S12 for $Au_{1289}$-$dOT_{251}$ NPs.

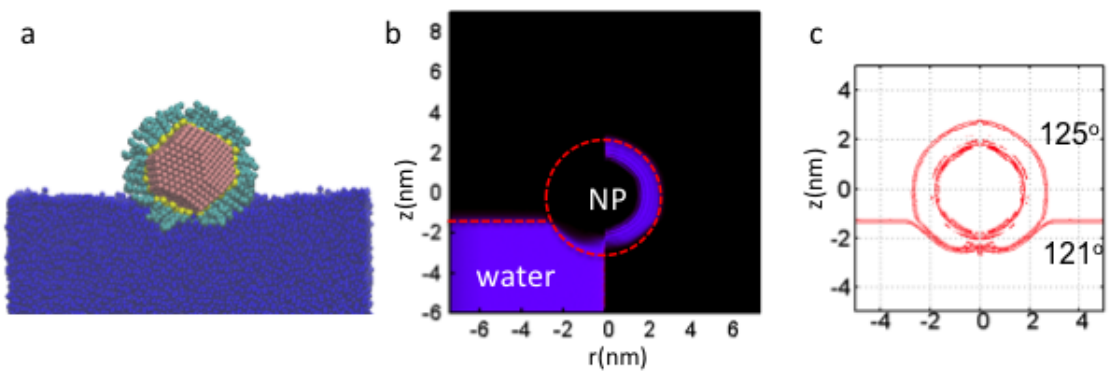


Figure S12: **a)** Snapshots of equilibrated configurations of $Au_{3832}$-$dOT_{476}$ (only atoms with y < 0 (y axis is normal to the plane) are represented). **b)** Density profile indicating the water level on the left and the ligands on the right. **c)** Contour lines and contact angles for the different particles investigated in this work. See text for further details.

### 4.2 Simulation of a monolayer at the interface

We have shown so far that the dependence of the computed contact angles with the amount of MHol molecules, i.e, dOT:MHol= 1:0, 0.5:0.5, agrees quantitatively and qualitatively with the experimental data. However, an important difference between our simulations and the experiments is that the latter are performed using close packed monolayers. To address the impact of nanoparticle-nanoparticle interactions (which are present in these monolayers) on the nanoparticle immersion and contact angles, we have performed additional simulations of $Au_{3832}$-$dOT_{476}$, $Au_{3832}$-$dOT_{238}$-$MHol_{238}$ nanoparticle arrays (see Figure S13).

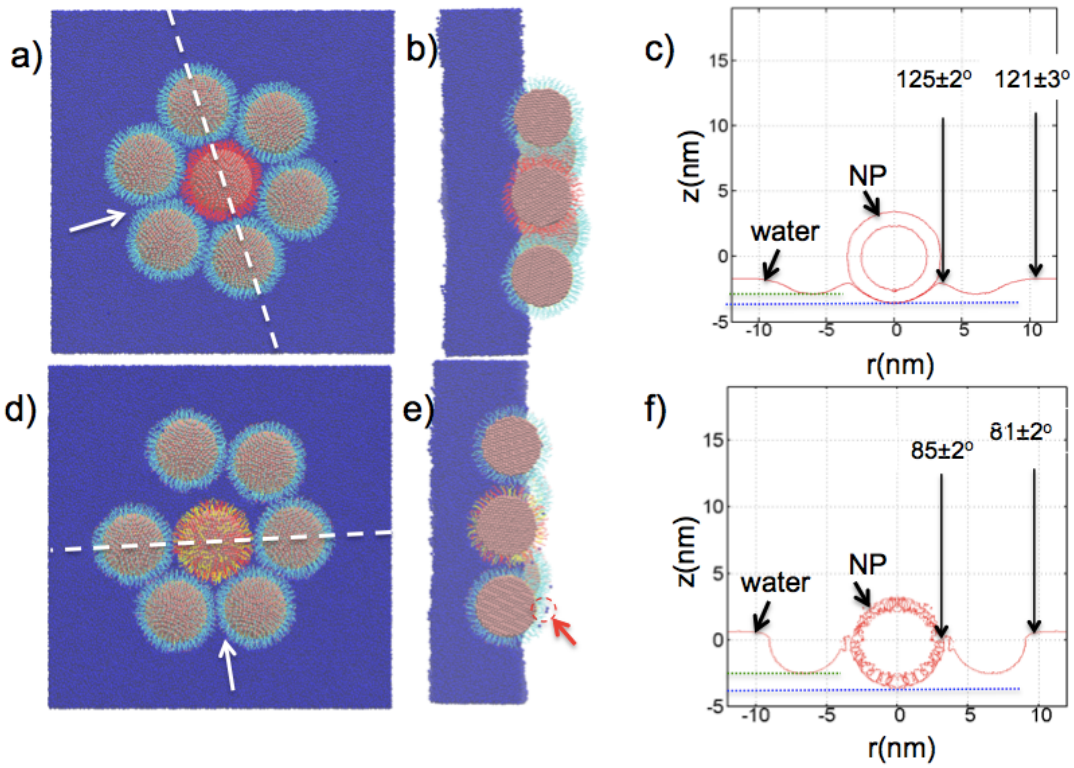


**Figure S13:** Representative snapshots of nanoparticle arrays consisting of 7 nanoparticles adsorbed at the water interface. Top (a and d) and side (b and c) views of $Au_{3832}$-$dOT_{476}$ nanoparticles and $Au_{3832}$-$dOT_{238}$-$MHol_{238}$ are shown. The ligands of the central particle in the array have been colored in red (dOT) and yellow (MHol). The panels represented in the view correspond to the plane defined by the dashed lines in a) and b). The arrows in these panels indicate the view direction. The red circle in Panel e) highlights the adsorption of water molecules at the top of the nanoparticles in the water vapor region. Panels c) and f) represent contour lines for both nanoparticles (NP) and water for the isochore 16 particles/nm$^3$. The green and blue horizontal lines highlight the different immersions of the central and outer particles with respect to the water surface at long r. We also show in panels c) and f) the contact angles estimated by taking two references for *h*.

Our simulations show that the dOT-functionalized particles tend to form close packed arrays, a behavior that is compatible with its hydrophobic character. For simulations spanning the same time scales we find that the MHol functionalized particles have a smaller tendency to form close packed arrays (cf. Fig.S13 a and d), again compatible with their hydrophilic character (see Figures 3-b and e) Our simulations show that the interactions with the neighboring particles result in the deformation of the thiol layer with the formation of planes with neighboring atoms. We do not find evidence for formation of thiol bundles in the dOT or in the MHol. (see Fig. S13 a,b, d and e). Our simulations also show that water molecules can adsorb on the particle surface exposed to the vapor region. This weak adsorption is promoted by the

formation of hydrogen bonds between water and the terminal group OH in the MHol thiol. We show in Figures 3-c) and f) contour plots obtained from the computation of the local density around the center of mass of the central particle using the cylindrical coordinates, r and z. We have replicated the r>0 plane in the r<0 one to provide a full view of the environment around the central particle. Interestingly we find that the immersion of the central particle with respect to the water surface position far from the particle is slightly larger than the immersion of the outer particle. This immersion differences show that the particles in the array experience a different wetting environment depending on their location. The immersion of the central particle is determined by an axially symmetric environment, where the particle interacts with water and other particles, while the outer particles interact with water too all along the cluster perimeter. We have estimated the contact angles for the central particle by using the same geometric construction introduced above for the isolated particles, but taking into account two values for *h*; (1) the height of the water surface next to the nanoparticle surface and (2) the height at long distances, *r*, from the nanoparticle surface, where the water density reaches a plateau (see Fig S13-f). The contact angles show a small sensitivity to the reference plane *h*, and are in good agreement with the estimates for the single particle. Our simulation results indicate that the contact angles measured in single particle or arrays different slightly, with the later being higher than the former. However the observed changes are small, and well within the uncertainty of our experiments, hence the experimental contact angles on monolayers provide a good approximation to the contact angle of isolated particles.

Finally we can estimate from our simulations the average particle-particle distance in the arrays, which gives information on the array lattice parameter, and the edge-to-edge distance which can be compared with our experimental model. For the particle-particle distance we find a value of 6.50±0.08 nm and 6.56±0.06 nm for $Au_{3832}$-$dOT_{476}$ and $Au_{3832}$-$dOT_{238}$-$MHol_{238}$ respectively. The edge-to-edge distance was computed by calculating the closest distance between attached neighboring particles. For the $Au_{3832}$-$dOT_{238}$-$MHol_{238}$, where the 7 particles do not form a close packed arrangement within the simulation timescale, we considered the distance between nanoparticles in direct contact. Our estimates for the edge-to-edge distance, 1.31 nm and 1.35 nm for $Au_{3832}$-$dOT_{476}$ and $Au_{3832}$-$dOT_{238}$-$MHol_{238}$ respectively, are in reasonable agreement with the experimental estimates (see Table 1 in the main text).

## 5. Sessile drop contact angle

Substrate: Glass substrates (cover slips) were cleaned with organic solvents and them with freshly prepared piranha solution. The substrate was rinsed with ultrapure water and dried with a nitrogen flux. For dOT the substrate was further functionalized with (3-mercaptopropyl)trimethoxysilane to avoid the detachment of the nanoparticles during the contact angle deposition.

Deposition: The deposition was performed using a Langmuir trough using a Langmuir-Schaefer method. The substrate was dried after deposition and the process was repeated 3 times to achieve a full coverage of the substrate.

Contact angle: The contact angle measurement was performed in a DSA100 instrument (Krüss, Germany). At least 10 drops of 4 μL were deposited on each substrate and the contact angle was averaged to all the angles.

## 6. References


1. K. A. Tay and F. Bresme, *Journal of the American Chemical Society*, 2006, **128**, 14166-14175.
2. K. Tay and F. Bresme, *Mol Simulat*, 2005, **31**, 515-526.